Dalton Transactions

## COMMUNICATION

Check for updates

Mechanochemical synthesis of iron aluminyl complexes†

Fabian Kallmeier, [iD] Aidan J. R. Matthews, [iD] Gareth R. Nelmes, [iD]
Nina R. Lawson [iD] and Jamie Hicks [iD] *

A series of iron aluminyl complexes have been synthesised in good crystalline yields from reactions between bulky diamido aluminium iodide complexes and K[Fe(CO)$_2$Cp] in the solid state. The series of metal–metal bonded complexes have been characterised by X-ray crystallography and were investigated using density functional theory to probe the effects of ligand substitution on the Al–Fe bond.

Mechanochemistry has been deemed a future direction of 'green chemistry'.[1] This is because reactions can be performed solvent-free (or near solvent-free), cheaper, safer, and often with less energy input than traditional solution-state chemistry.[1,2] Mechanochemistry is already widely used in many areas of chemistry[3] but has only recently started to make an impact in main group synthesis.[4–11] Some examples of note include Kubota, Ito and co-workers 2021 report that Grignard reagents can be synthesised mechanochemically in high yields (Fig. 1, **I**).[12] Furthermore, the Grignard 'paste' isolated from the mill reacted mechanochemically with a range of electrophiles typical of Grignard reagents. In 2022, Harder and co-workers showed that magnesium radical complexes could be synthesised by the mechanochemical reduction of magnesium iodide precursor complexes with potassium-coated KI (**II**).[13,14] Last year, García, García-Álvarez and co-workers reported a fast, scalable and solvent-free method to access the commonly named "Lappert's heavier tetrylenes" E[N(SiMe$_3$)$_2$]$_2$ (E = Ge, Sn, Pb) by a mechanochemical synthesis (**III**).[15] Earlier this year Yamashita and co-workers also reported that non-solvated dialkylaluminyl anion can be isolated from the mechanochemical reduction of the dialkylaluminium iodide with an Na/K alloy (**IV**).[16]

In terms of using mechanochemical reactions in the synthesis of metal–metal bonded compounds, results in the literature are scarce. Harder and co-workers recently showed that Mg(ı)–Mg(ı) bonded dimers can be synthesised through the mechanochemical reduction of β-diketiminate magnesium
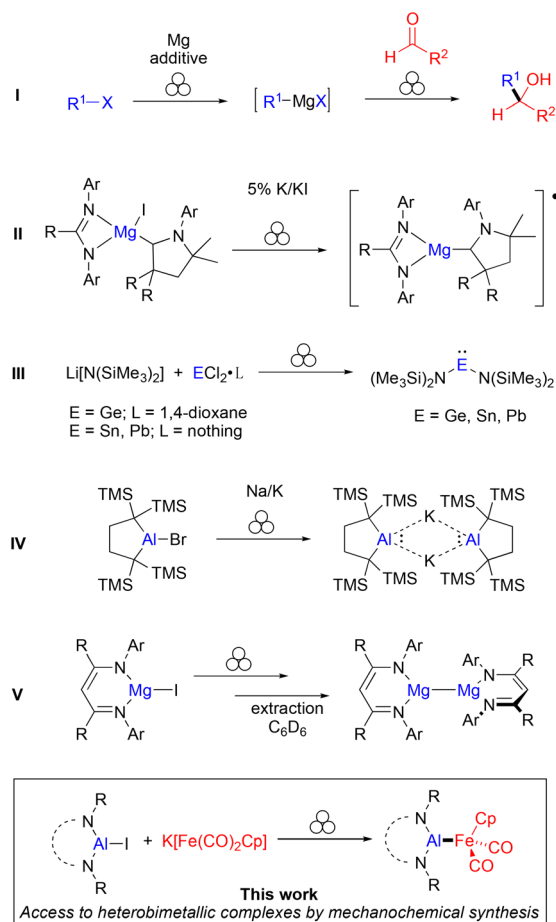
Fig. 1 Selected main group mechanochemical reactions. Ar = aryl, TMS = trimethylsilyl, R/R^1/R^2 = various organic groups.

*Research School of Chemistry, Australian National University, ACT, 2601, Australia.
E-mail: jamie.hicks@anu.edu.au*

iodide compounds (Fig. 1, **V**).[17] However, the group proposed that the Mg–Mg bond was likely formed upon extraction into C_6D_6 *via* radical dimerisation. In this work, we build on these recent reports showing that mechanochemical synthesis can be used in the preparation of heterobimetallic complexes with unsupported metal–metal bonds.

Six diamido aluminium iodide complexes were used as precursors in this work, four bearing xanthene-based diamido ligands ([^{Dipp}**NON**]$^{2-}$, [^{tBuDipp}**NON**]$^{2-}$, [^{tBu}**NON**]$^{2-}$, [^{TIPS}**NON**]$^{2-}$), one bearing a diamidosilyl ligand, [**DAS**]$^{2-}$, and one bearing two monodentate amido ligands [**Dipp(TIPS)N**]$^{-}$ for an acyclic comparison (Scheme 1).[18] The four xanthene-based ligands all feature the same 2,7-di-*tert*-butyl-9,9-dimethylxanthene scaffold and vary only by the substituents on the nitrogen donors. (^{Dipp}**NON**)**AlI** and [**Dipp(TIPS)N**]$_2$**AlI** have been reported previously,[19,20] but (^{TIPS}**NON**)**AlI**, (^{tBuDipp}**NON**)**AlI**, (^{tBu}**NON**)**AlI** and (**DAS**)**AlI** are reported as part of this work (see ESI† for synthesis and characterising data).

With the range of aluminium iodide compounds in hand, our attention turned to the synthesis of the iron aluminyl complexes. A number of iron aluminyl complexes have previously been reported,[21] all synthesised in the solution phase through reactions between bulky aluminium (di)halide complexes and the [$Fe(CO)_2Cp$]$^{-}$ (Fp) anion (either the Na or K salt). Taking inspiration from these previous studies, the reaction between (^{TIPS}**NON**)**AlI** and K[Fp] in benzene was investigated.

Monitoring the reaction by ^1H NMR spectroscopy, it was determined that after stirring the suspension for 16 hours at room temperature, the reaction only saw 51% conversion to the iron aluminyl complex. Stirring the reaction for another 2 days led to complete conversion to the desired iron aluminyl complex (^{TIPS}**NON**)**AlFp**. In comparison, the addition of the same reagents (0.25 mmol scale) as solids into an IKA Ultra-Turrax Tube Drive fitted with a 20 mL ball mill tube, 30 stainless steel balls and 258 mg of graphite as flux, saw complete conversion within one hour of milling. Upon workup, this gave (^{TIPS}**NON**)**AlFp** in a 79% yield (Scheme 1). A similar procedure was used in the synthesis of (^{tBuDipp}**NON**)**AlFp**, (^{tBu}**NON**)**AlFp**, (^{Dipp}**NON**)**AlFp** and (**DAS**)**AlFp**, which upon workup, all gave moderate to good crystalline yields of the iron aluminyl complexes (33–68%). Unfortunately, even after multiple attempts in both solution and the solid state, the reaction between the acyclic precursor [**Dipp(TIPS)N**]$_2$**AlI** and K[Fp] led to decomposition in every case, yielding a complex mixture of products by ^1H NMR spectroscopy.

The five iron aluminyl complexes have been characterised by X-ray crystallography, and their solid-state structures are shown in Fig. 2. All five complexes have similar solid-state structures, bearing an unsupported Al–Fe bond between a diamidoaluminium fragment and the $Fe(CO)_2Cp$ moiety. However, upon closer inspection, the solid-state structures reveal some interesting trends. Firstly, comparing the four **NON**-coordinated complexes, the Al–Fe bond length shortens from 2.4356(8) Å in (^{TIPS}**NON**)**AlFp** to 2.3860(5)/2.3854(5) Å in (^{tBuDipp}**NON**)**AlFp**/(^{Dipp}**NON**)**AlFp**, with that of (^{tBu}**NON**)**AlFp** in between at 2.4085(11) Å (Table 1).

As the difference in Al–Fe bond length could be a consequence of sterics, a comprehensive analysis of the steric profiles of all five ligands, using both SambVca 2.1 (% buried
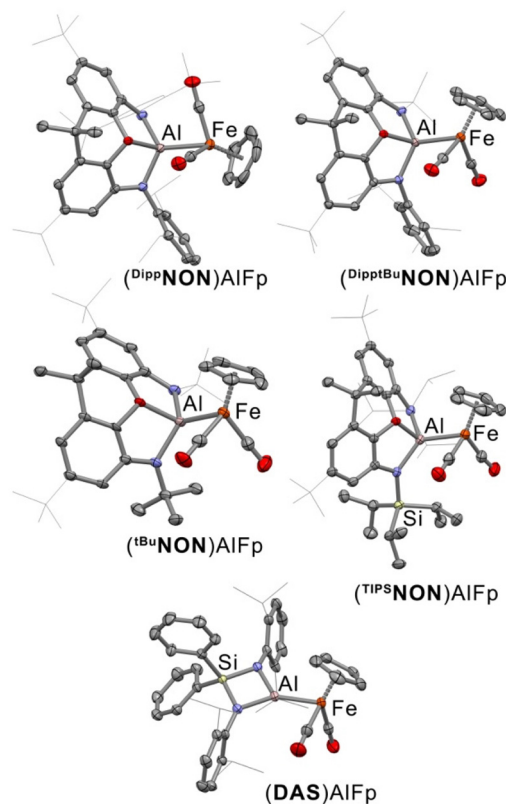
Scheme 1 Mechanochemical synthesis of the five iron aluminyl complexes.
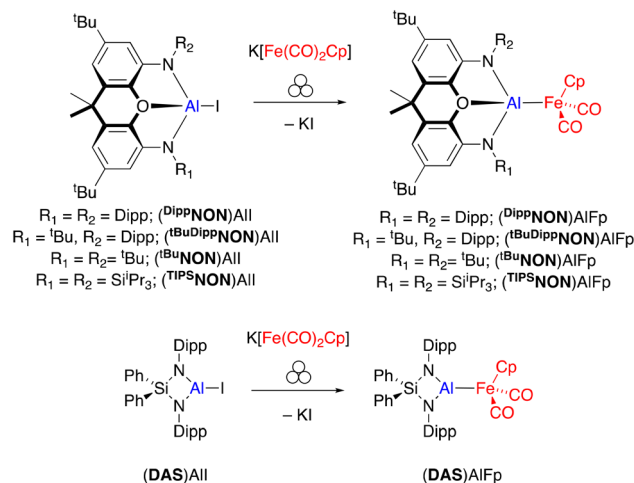
Fig. 2 Solid-state structures of (^{Dipp}**NON**)**AlFp** (top-left), (^{tBuDipp}**NON**)**AlFp** (top-right), (^{tBu}**NON**)**AlFp** (middle-left), (^{TIPS}**NON**)**AlFp** (middle-right) and (**DAS**)**AlFp** (bottom) as determined by single-crystal X-ray crystallography. Displacement ellipsoids set at the 50% probability level. Hydrogen atoms have been omitted and selected organic groups have been shown in wireframe for clarity.

Table 1 Selected bond lengths and angles of the iron aluminyl complexes

	Al–Fe (Å)	Al–O (Å)	O–Al–Fe (°)	N···N (Å)
($^{\text{DiPP}}$NON)AlFp	2.3854(5)	1.9577(11)	113.23(4)	3.247(2)
($^{\text{tBuDiPP}}$NON)AlFp	2.3860(5)	1.9204(10)	110.95(3)	3.289(2)
($^{\text{tBu}}$NON)AlFp	2.4087(10)	1.915(2)	107.08(7)	3.308(4)
($^{\text{TIPS}}$NON)AlFp	2.4356(8)	1.9142(18)	101.66(6)	3.384(4)
(DAS)AlFp	2.2884(7)	—	—	—

volume) and AtomAccess (% accessible surface area),[22,23] was conducted. Both methods were unanimous in the ordering of the ligands in terms of sterics, finding the following trend: $^{\text{tBu}}$**NON** < **DAS** < $^{\text{tBuDiPP}}$**NON** < $^{\text{TIPS}}$**NON** < $^{\text{DiPP}}$**NON** (see ESI† for further details). This ordering does appear to correlate with the measured Al–Fe bond length of the complexes; therefore, it can be concluded that sterics alone cannot be responsible for the differences in structures. Returning to the solid-state structures of the four Al–Fe **NON**-complexes, trends mirroring those of Al–Fe bond length can also be seen in the O–Al bond length, O–Al–Fe angle and N···N separation (Table 1). Together, these observations show that moving from ($^{\text{DiPP}}$**NON**)**AlFp** to ($^{\text{TIPS}}$**NON**)**AlFp**, the Al centre is being "pulled" further into the tridentate **NON**-binding pocket (as is seen by the decreasing Al–O length), increasing N···N separation and reducing the O–Al–Fe angle.

In an attempt to rationalise the observed trend in terms of electronics, the series of iron aluminyl complexes was investigated using density functional theory (DFT). The geometry of all five complexes was optimised at the PBE0-D3BJ/BS1 level of theory. The optimised geometries are in good agreement with the single-crystal X-ray data, producing the same ordering of Al–Fe bond lengths (Table 2) as observed in the solid-state (see ESI† for further details).[24] As expected, all five iron aluminyl complexes display similar electronic structures: in every case, the HOMO and HOMO−1 are **NON**/**DAS** ligand-based orbitals, which include electron density from the nitrogen lone pairs. In the four **NON** complexes, the HOMO−2 corresponds to the Al–Fe σ-bonding orbital, which is a similar energy for ($^{\text{DiPP}}$**NON**)**AlFp**, ($^{\text{tBuDiPP}}$**NON**)**AlFp** and ($^{\text{tBu}}$**NON**)**AlFp** (−6.56 to −6.55 eV), but slightly higher for ($^{\text{TIPS}}$**NON**)**AlFp** (−6.53 eV) due to the significantly more σ-donating N-bound TIPS groups. This orbital for the ($^{\text{tBu}}$**NON**)**AlFp** complex is shown in Fig. 3. In the (**DAS**)**AlFp** complex, the equivalent orbital is much
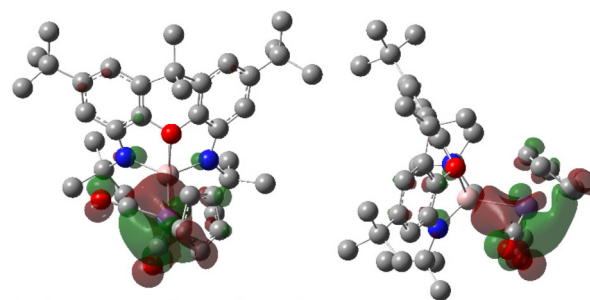
Fig. 3 Molecular orbital (HOMO−2) of the σ(Fe−Al) bond between ($^{\text{tBu}}$NON)AlFp, showing approximate sigma symmetry along the Al−Fe axis. Hydrogen atoms omitted for clarity, and MO rendered with an iso-value of 0.035 e⁻ Å⁻³. Aluminium atom depicted in pale pink and iron atom in purple.

lower in energy at −7.87 eV and corresponds to the HOMO−12. In all compounds, three iron-based molecular orbitals that are high in d-character can be located between HOMO−5 and HOMO−13, which are all polarised towards the Al centre.

To gain further insight into the Al–Fe bond, the series was additionally investigated using natural bond orbital (NBO) analysis, with a summary of the findings is presented in Table 2. The NBO corresponding to the σ(Fe–Al) bond is similar in all five complexes, containing significant contributions from the 3d(Fe) and 3s(Al) orbitals and are polarised toward the iron centre (see ESI† for further details). The calculated Al–Fe bond index is similar in all complexes, ranging from 0.35–0.39. This is consistent with that calculated for previously reported iron-aluminyl complexes,[21] and therefore shows a significant ionic contribution to the bond. The natural population analysis (NPA) charge on the Al centre (Q_{Al}) also follows the same trend as the Al–Fe bond lengths, with the Al centre in ($^{\text{DiPP}}$**NON**)**AlFp** calculated to have the largest positive charge (+1.88) and that in ($^{\text{TIPS}}$**NON**)**AlFp** and ($^{\text{tBu}}$**NON**)**AlFp** to have the smallest (+1.82) of the four **NON** complexes (Table 2). The three-coordinate (**DAS**)**AlFp** was found to have the lowest Q_{Al} of the series at +1.73. In comparison, the charge on Fe (Q_{Fe}) remains much more consistent across the series (−0.43 to −0.47). ($^{\text{DiPP}}$**NON**)**AlFp** has the largest difference in Q_{Al} and Q_{Fe} and is consequently the **NON**-complex with the shortest Al–Fe bond. The differences observed in the **DAS** complex can be attributed to the different coordination environment at aluminium and significantly different N–Al–N bite angle, increasing the Al-s character of the bonding orbital.[25]

As an interesting final note to this study, in the mechanochemical reaction between ($^{\text{DiPP}}$**NON**)**AlI** and K[Fp], a small (<2%) but reproducible side-product was observed. This was most noticeable during the crystallisation of the (colourless) complex ($^{\text{DiPP}}$**NON**)**AlFp**, which frequently produced a few small, red crystals alongside the primary colourless crystals of ($^{\text{DiPP}}$**NON**)**AlFp**. X-ray crystallographic analysis of this side-product revealed it to be [{($^{\text{DiPP}}$**NON**)AlOC(μ-FeCp)}₂], a carbyne-bridged diiron complex with two ($^{\text{DiPP}}$**NON**)**Al** moieties bound to the oxygen atoms of the former carbonyl ligands

Table 2 Summary of the key findings from DFT and NBO analysis of the five iron aluminyl complexes

	Al–Fe bond length (Å)	Bond index	NPA charge Q_{Al}	NPA charge Q_{Fe}
($^{\text{TIPS}}$NON)AlFp	2.390	0.373	+1.821	−0.443
($^{\text{tBu}}$NON)AlFp	2.363	0.357	+1.816	−0.447
($^{\text{tBuDiPP}}$NON)AlFp	2.352	0.350	+1.840	−0.430
($^{\text{DiPP}}$NON)AlFp	2.326	0.349	+1.881	−0.468
(DAS)AlFp	2.285	0.393	+1.732	−0.466

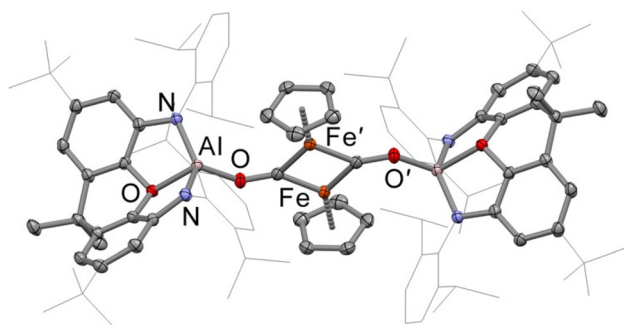**Fig. 4** Solid state structures of [{(^{DiPP}NON)AlOC(μ-FeCp)}$_2$] as determined by single-crystal X-ray crystallography. Displacement ellipsoids set at the 50% probability level. Hydrogen atoms have been omitted and selected organic groups have been shown in wireframe for clarity.

(Fig. 4). The compound is isostructural to the boron analogue recently reported by us[26] and similar to the benzylidyne-bridged diiron complex previously reported by Sitzmann and co-workers.[27] It can be envisioned that [{(^{DiPP}NON)AlOC(μ-FeCp)}$_2$] may be formed from the iron aluminyl complex (^{DiPP}NON)AlFp, by simple loss of a carbonyl ligand from each iron centre and dimerisation. However, all attempts to convert (^{DiPP}NON)AlFp into the carbyne complex (refluxing the complex in various solvents and/or irradiation with UV light) either led to no reaction or decomposition of the (^{DiPP}NON)AlFp. It is therefore proposed that the complex is formed in the milling of (^{DiPP}NON)AlI and K[Fp], by initial nucleophilic attack of one of the Fp carbonyl ligands on the electrophilic Al centre. Nucleophilic reactivity of the [Fp]$^-$ carbonyl ligands has been previously reported,[28] and a similar mechanism was proposed for the boron analogue.[26]

Conclusions

In conclusion, we have successfully synthesised a series of iron aluminyl complexes *via* mechanochemical methods using bulky diamido aluminium iodide complexes and K[Fe(CO)$_2$Cp] in the solid state. These complexes were characterised by X-ray crystallography, revealing significant structural insights into the Al–Fe bonding environment. Density functional theory (DFT) calculations further elucidated the electronic structure and bonding interactions, highlighting the influence of ligand substitution on the Al–Fe bond length and the nature of the Al centre. Our findings underscore mechanochemistry as a powerful tool for accessing heterobimetallic complexes with unsupported metal–metal bonds, paving the way for future advancements in main group and transition metal synthesis.

Data availability

The data supporting this article have been included as part of the ESI.† Finalised CIFs for all X-ray diffraction structures

(2359911–2359919)† have been deposited at the Cambridge Crystallographic Data Centre.

Conflicts of interest

There are no conflicts to declare.

Acknowledgements

References

1 K. J. Ardila-Fierro and J. G. Hernández, *ChemSusChem*, 2021, **14**, 2145.

2 (*a*) T. Friščić, C. Mottillo and H. M. Titi, *Angew. Chem., Int. Ed.*, 2020, **59**, 1018; (*b*) J.-L. Do and T. Friščić, *ACS Cent. Sci.*, 2017, **3**, 13.

3 See for example: (*a*) X. Liu, Y. Li, L. Zeng, X. Li, N. Chen, S. Bai, H. He, Q. Wang and C. Zhang, *Adv. Mater.*, 2022, **34**, 2108327; (*b*) A. Krusenbaum, S. Grätz, G. T. Tigineh, L. Borchardt and J. G. Kim, *Chem. Soc. Rev.*, 2022, **51**, 2873; (*c*) J. L. Howard, Q. Cao and D. L. Browne, *Chem. Sci.*, 2018, **9**, 3080.

4 (*a*) D. Tan and F. Garcia, *Chem. Soc. Rev.*, 2019, **48**, 2274; (*b*) N. R. Rightmire and T. P. Hanusa, *Dalton Trans.*, 2016, **45**, 2352.

5 D. W. Peters and R. B. Blair, *Faraday Discuss.*, 2014, **170**, 83.

6 N. C. Boyde, N. R. Rightmire, T. P. Hanusa and W. W. Brennessel, *Inorganics*, 2017, **5**, 36.

7 R. F. Koby, A. M. Doerr, N. R. Rightmire, N. D. Schley, B. K. Long and T. P. Hanusa, *Angew. Chem., Int. Ed.*, 2020, **59**, 9542.

8 N. Davison, J. A. Quirk, F. Tuna, D. Collison, C. L. McMullin, H. Michaels, G. H. Morritt, P. G. Waddell, J. A. Gould, M. Freitag, J. A. Dawson and E. Lu, *Chem*, 2023, **9**, 576.

9 Y. Gao, K. Kubota and H. Ito, *Angew. Chem., Int. Ed.*, 2023, **62**, e202217723.

10 J. V. Nallaparaju, R. Satsi, D. Merzhyievskyi, T. Jarg, R. Aav and D. G. Kananovich, *Angew. Chem., Int. Ed.*, 2024, **63**, e202319449.

11 M. Glavinović, M. Krause, L. Yang, J. A. McLeod, L. Liu, K. M. Baines, T. Friščić and J.-P. Lumb, *Sci. Adv.*, 2017, **3**, e1700149.

12 R. Takahashi, A. Hu, P. Gao, Y. Gao, Y. Pang, T. Seo, J. Jiang, S. Maeda, H. Takaya, K. Kubota and H. Ito, *Nat. Commun.*, 2021, **12**, 6691.

13 D. Jędrzkiewicz, J. Mai, J. Langer, Z. Mathe, N. Patel, S. DeBeer and S. Harder, *Angew. Chem., Int. Ed.*, 2022, **61**, e202200511.

14 J. Hicks, M. Juckel, A. Paparo, D. Dange and C. Jones, *Organometallics*, 2018, **37**, 4810.

15 J. A. Cabeza, J. F. Reynes, F. García, P. García-Álvarez and R. García-Soriano, *Chem. Sci.*, 2023, **14**, 12477.

16 S. Kurumada, R. Yamanashi, K. Sugita, K. Kubota, H. Ito, S. Ikemoto, C. Chen, T. Moriyama, S. Muratsugu, M. Tada, T. Koitaya, T. Ozaki and M. Yamashita, *Chem. – Eur. J.*, 2024, **30**, e202303073.

17 D. Jędrzkiewicz, J. Langer and S. Harder, *Z. Anorg. Allg. Chem.*, 2022, **648**, e202200138.

18 (*a*) C. A. Cruz, D. J. H. Emslie, C. M. Robertson, L. E. Harrington, H. A. Jenkins and J. F. Britten, *Organometallics*, 2009, **28**, 1891; (*b*) A. Nicolay, M. S. Ziegler, L. Rochlitz and T. D. Tilley, *Polyhedron*, 2020, **180**, 114420; (*c*) R. Murugavel, N. Palanisami and R. J. Butcher, *J. Organomet. Chem.*, 2003, **675**, 65; (*d*) B. Shen, L. Ying, J. Chen and Y. Luo, *Inorg. Chim. Acta*, 2008, **361**, 1255.

19 J. Hicks, P. Vasko, J. M. Goicoechea and S. Aldridge, *Nature*, 2018, **557**, 92.

20 R. A. Jackson, A. J. R. Matthews, P. Vasko, M. F. Mahon, J. Hicks and D. J. Liptrot, *Chem. Commun.*, 2023, **59**, 5277.

21 (*a*) T. Agou, T. Yanagisawa, T. Sasamori and N. Tokitoh, *Bull. Chem. Soc. Jpn.*, 2016, **89**, 1184; (*b*) I. M. Riddlestone, J. Urbano, N. Phillips, M. J. Kelly, D. Vidovic, J. I. Bates, R. Taylor and S. Aldridge, *Dalton Trans.*, 2013, **42**, 249; (*c*) C. Jones, S. Aldridge, T. Gans-Eichler and A. Stasch, *Dalton Trans.*, 2006, 5357; (*d*) T. Yanagisawa, Y. Mizuhata and N. Tokitoh, *Heteroat. Chem.*, 2018, **29**, e21465; (*e*) B. N. Anand, I. Krossing and H. Noth, *Inorg. Chem.*, 1997, **36**, 1979; (*f*) H. Braunschweig, J. Muller and B. Ganter, *Inorg. Chem.*, 1996, **35**, 7443; (*g*) I. M. Riddlestone, S. Edmonds, P. A. Kaufman, J. Urbano, J. I. Bates, M. J. Kelly, A. L. Thompson, R. Taylor and S. Aldridge, *J. Am. Chem. Soc.*, 2012, **134**, 2551; (*h*) R. A. Fischer and T. Priermeier, *Organometallics*, 1994, **13**, 4306; (*i*) K. Nakaya, A. Ishii and N. Nakata, *Mendeleev Commun.*, 2022, **32**, 71; (*j*) S. Sinhababu, M. R. Radzhabov, J. Telser and N. P. Mankad, *J. Am. Chem. Soc.*, 2022, **144**, 3210.

22 L. Falivene, Z. Cao, A. Petta, L. Serra, A. Poater, R. Oliva, V. Scarano and L. Cavallo, *Nat. Chem.*, 2019, **11**, 872.

23 G. K. Gransbury, S. C. Corner, J. G. C. Kragskow, P. Evans, H. M. Yeung, W. J. A. Blackmore, G. F. S. Whitehead, I. J. Vitorica-Yrezabal, N. F. Chilton and D. P. Mills, *J. Am. Chem. Soc.*, 2023, **145**, 22814.

24 Y. Minenkov, Å. Singstad, G. Occhipinti and V. R. Jensen, *Dalton Trans.*, 2012, **41**, 5526.

25 J. Hicks, P. Vasko, J. M. Goicoechea and S. Aldridge, *Angew. Chem., Int. Ed.*, 2021, **60**, 1702.

26 E. E. Nahon, G. R. Nelmes, P. J. Brothers and J. Hicks, *Chem. Commun.*, 2023, **59**, 14281.

27 G. Y. Vollmer, M. W. Wallasch, D. Saurenz, T. R. Eger, H. Bauer, G. Wolmershäuser, M. H. Prosenc and H. Sitzmann, *Organometallics*, 2015, **34**, 644.

28 See for example: (*a*) T. Pugh, N. F. Chilton and R. A. Layfield, *Angew. Chem., Int. Ed.*, 2016, **55**, 11082; (*b*) M. P. Blake, N. Kaltsoyannis and P. Mountford, *Chem. Commun.*, 2013, **49**, 3315.